International Journal of Impact Engineering 213 (2026) 105657

Contents lists available at ScienceDirect

International Journal of Impact Engineering

journal homepage: www.elsevier.com/locate/ijimpeng

Water impact of flexible aluminum panels: Experimental study and numerical validation across different angles for aircraft ditching applications

Alessandro Giustina [a,*], Ivan Colamartino [b], Stefano Dolci [c], Marco Anghileri [a]

[a] Department of Aerospace Science and Technology, Politecnico di Milano, Via La Masa, 34, Milano, 20156, Italy
[b] Department of Mechanical Engineering, Politecnico di Milano, Via La Masa, 1, Milano, 20156, Italy
[c] Center for Collision Safety and Analysis, George Mason University, 4087 University Dr., Fairfax (VA), 22030, USA

ARTICLE INFO

Keywords:
Ditching
S-ALE
Wedged water impacts
Penalty factor
Fluid-structure interaction

ABSTRACT

Ditching behavior is typically studied using either high-stiffness representative structures or excessively complex assemblies replicating case studies of very specific aeronautical structures. The present study aims to investigate a comprehensive approach to ditching analysis, assessing experimentally and numerically the water impact behavior of thin flexible aeronautical-grade aluminum panels (Al 2024 T3), focusing on the influence of various test parameters, including panel thickness, angle of impact, ballast mass, and impact velocity. The panels were mounted on three different test fixtures, depending on the desired impact angles (0°, 15°, and 30°, with the last two being in a wedge configuration), obtaining high repeatability of acceleration and strain measures. A numerical finite element model for ditching applications was enhanced exploiting the structured arbitrary Lagrangian Eulerian (S-ALE) method, allowing for improved leakage control. Sensitivity studies were performed to assess the effect of mesh size and water domain dimensions. The fluid-structure interaction between Lagrangian and ALE domains was correlated with experimental data using quantitative curve comparison metrics. This allowed us to choose the best fitting penalty factor curve to be used in the numerical model. The final model was validated against the experimental results across a wide range of configurations, accurately capturing both acceleration peaks and strain gauge responses. The validated numerical framework has the potential to be used for the creation of a comprehensive robust database of ditching events, paving the way to future development of efficient, data-driven simplified numerical tools for early-stage aircraft design.

1. Introduction

Ditching is defined in aeronautics as the procedure of emergency landing of an aircraft on water, carried out when reaching an airfield is not possible. Although the impact may be generally less severe than ground emergency landing, the load distribution is completely different. In fact, upon impact, the fluid pressure is distributed uniformly normal to the skin panels of the fuselage, which are usually characterized by low thickness. In the case of a damage to one of these panels, the pressure loads are no longer evenly transmitted to the energy-absorbing components (bulkheads and frames), and the buoyancy of the fuselage is compromised [1]. Water impacts are burdened by a fatality rate between 26 and 34 % [2,3]; in particular, death by drowning after the actual ditching event is generally caused by the rapid sinking of the aircraft, which is highly affected not only by the integrity of the fuselage, but also by the position of the center of gravity and by the effectiveness of the emergency flotation systems (EFS) [4,5].

Manufacturers typically assess ditching kinematics and flotation through model-scale testing [6–8], which, however, is a method unable to accurately reproduce the deformability of the structures [9,10] or cavitation and ventilation effects [11]. On the other hand, full-scale testing with representative deformable models is remarkably expensive and only rarely used in the final stages of aircraft design or for validation purposes [12,13]. In addition, ditching compliance may be supported by structural comparison with similar designs already certified [14], though this approach cannot be applied to novel aircraft configurations, which may have different ditching behavior [15]. For these reasons, recently, industry and researchers are showing increasing interest in the use of numerical simulations in order to predict the outcome of water landing [16].

The problem of fluid–structure interaction (FSI) is very complex and computationally difficult to solve due to the large deformations of the water volume during the impact and the relatively long duration of the

* Corresponding author.
E-mail address: alessandro.giustina@polimi.it (A. Giustina).

https://doi.org/10.1016/j.ijimpeng.2026.105657
Received 2 July 2025; Received in revised form 6 January 2026; Accepted 18 January 2026
Available online 6 February 2026

event (up to a few seconds). Therefore, so far, many computational methods have been proposed. Finite volume methods (FVM) allow accurate prediction of the distribution of the hydrodynamic pressure on the aircraft [17–19], but they often neglect the coupling with structural deformations, which has been demonstrated to be essential in order to accurately calculate ditching loads and to evaluate fuselage integrity [10,20]. Commercial softwares based on finite element methods (FEM) are able to take into account FSI in ditching simulations of aeronautical structures. In fact, *Bisagni et al.* [21] and *Anghileri et al.* [22] conducted thorough analyses of different modeling strategies both based on Eulerian and meshless methods, validating them in cases of vertical drops into water respectively of a rigid sphere and a flexible panel. However, these studies were limited to impacts parallel to the water surface. Pure Lagrangian approach was found to be robust and efficient in preprocessing and model creation, but its accuracy is limited by the large fluid deformations. Arbitrary Lagrangian Eulerian (ALE) approach provided good correlation results and overall high computational efficiency, with accuracy driven by the choice of appropriate coupling parameters for the FSI. To mitigate computational problems due to mesh distortion, meshless methods have been extensively studied in literature, mainly for rigid bodies, based on smoothed particle hydrodynamics (SPH) theory, with promising results [21,23]. Main challenges, however, still include the calibration of particle density, the increased computational expense compared to mesh-based methods, and the difficulties in capturing viscous boundary layers, tangential shear stresses, and suction forces [24,25]. To reduce the high computational cost, hybrid methods have also been adopted for deformable structures, using SPH in proximity of the impact zone and FEM at the boundaries [26,27].

Due to the complexity of ditching events and of the understanding of its outcomes, experimental validation is however necessary to calibrate the numerical simulations. Ditching studies of complete aircraft models [12,28] provided exceptional insights into the understanding of this aspect of aircraft crashworthiness, but may have limited applicability to novel aircraft configurations. A comprehensive experimental dataset of ditching tests on representative specimens of airplane fuselage of different shapes (flat, curved, double-curved) and in different impact conditions was collected during the EU-funded research projects SMAES (SMart Aircraft in Emergency Situation) (2011–2014) and SARAH (Increased safety and robust certification for ditching of aircraft and helicopters) (2016–2020) [5]. These projects mainly focused on airplanes, reproducing realistic horizontal and vertical velocities typical of fixed-wing ditching [20]. Many literature studies focused instead on vertical water impact tests, which are more closely related to helicopter ditching conditions. However, most of them used panels with low flexibility [29–33] or tested panels in a narrow set of inclination angles [22,31,32,34–40].

Due to the huge computational effort needed to tackle the outstanding challenges in the ditching field, recently, interest is growing on simplified modeling strategies, ready to be integrated in the industrial process [41]. *Leon Muñoz et al.* [42,43] developed a multidisciplinary process chain for the design phase of new aircraft configurations, integrating a proprietary FE code based on a hybrid Lagrangian-meshless approach. *Schwarz et al.* [44], instead, exploited novel computational methods based on machine learning to consider structural deformations in the prediction of ditching loads.

In this context, the present article aims to obtain a comprehensive simulation method to study the ditching of aeronautical flexible panels belonging to helicopter structures, through the validation of a high-fidelity FEM model on experimental tests of thin aluminum panels impacting water vertically in a large variety of impact conditions. Three angles configurations were investigated (0°, 15° and 30°, with the last two being mounted on wedged fixtures). These data were used to validate a FE numerical model based on the structured arbitrary Lagrangian Eulerian (S-ALE) formulation. The numerical model, correlated with a large range of impact configurations, can serve as a foundation for an extensive and reliable simulation database, supporting the development and validation of a new set of tools for ditching analysis.

2. Materials and methods

2.1. Experimental tests

Aeronautical grade Al 2024 T3 panels were used, resembling the layout of many aircraft models still in operation, with a yield strength of 335 MPa and a failure strain of 26% [45]. Two different thickness values were investigated: $t = 1$ mm and $t = 1.6$ mm. Three different test fixtures were used to support the aluminum panels depending on the desired inclination angle with respect to the water surface. The fixture used for tests at 0°, illustrated in Fig. 1(b) was a solid aluminum frame with internal square opening measuring 280 × 280 mm, enclosed by aluminum panels (3 mm thick), reinforced by L-shaped profiles at the corners. The aluminum panels were fixed to the frame by a total of 32 bolts, 8 for each side, positioned at 160 mm from the center of the panel [22] (Fig. 1(a)). The other two fixtures for guiding the panels during the fall were manufactured as steel welded structures in wedge configurations of 150° and 120° (considering an angle of incidence of each single panel respectively of 15° and 30°, illustrated in Figs. 1(c) and 1(d)). The wedged shape was chosen in order to obtain a symmetric structure and minimize lateral loads during the impact. The portions of the wedges where the panels were mounted were dimensionally consistent with those of the frame used for 0° tests (Fig. 1(a)). These two test fixtures were manufactured using steel square tubes with a thickness of 4 mm and steel plates with thickness of 10 mm to reinforce the structure.

A circular water basin of 1.5 m in diameter width and 1 m in depth was used to investigate water impacts. Hence, the dimensions of the panels (400 × 400 mm) were chosen in order not to be influenced by wave reflection effects, at least for the time span relevant to the impact phase. Due to the limited depth of the water basin, rubber tires were used to stop the fall of the test articles before hitting the bottom of the pool, carefully verifying that this did not to interfere with the time span of interest for the measurement of forces and deformations during the water impact.

Two orthogonal high-speed cameras were used to ensure correct impact angle and velocity, one with frontal view and the other one with lateral view (Figs. 2(a), 2(b) and 2(c)). The whole experimental setup is illustrated in Fig. 2(d), highlighting the positioning of the cameras.

Four piezoresistive accelerometers EGCS-D0-250 by Measurement Specialties™ were positioned at the corners of the fixtures, as illustrated in Fig. 2(a), in order to measure vertical acceleration data. The acceleration data were filtered following SAEJ211 regulation with filter CFC180 (four-poles phaseless filter with a cutoff frequency of 300 Hz). In two of the tests performed with the 30° wedge fixture, one of the two panels was equipped with 8 strain gauges (KYOWA KFGS-3-350), positioned on the main diagonals of the panel, at distances of 50 mm and 110 mm from the center of the panel, as illustrated in Fig. 3. These strain data were used for additional correlation with numerical simulations and were used only in 30° tests, given the lower expected strain values, to avoid the risk of detachment of the sensors.

A summary of the experimental tests performed, with respective configurations, is reported in Table 1. For each impact configuration, two tests were performed, with the exception of the two tests at lower impact speed (A3_30_m1_v2 and A4_30_m2_v2). The maximum velocity achievable was limited by the necessity of performing experimental tests inside the laboratory and using its bridge crane.

2.2. Numerical methods

ALE method was chosen for numerical simulations in the present work due to its versatility in the calibration of FSI and to its computational efficiency with respect to other methods, as already mentioned in the Introduction.

In general, ALE is a hybrid method between the Lagrangian formulation, in which the mesh follows the motion of the material, suffering,

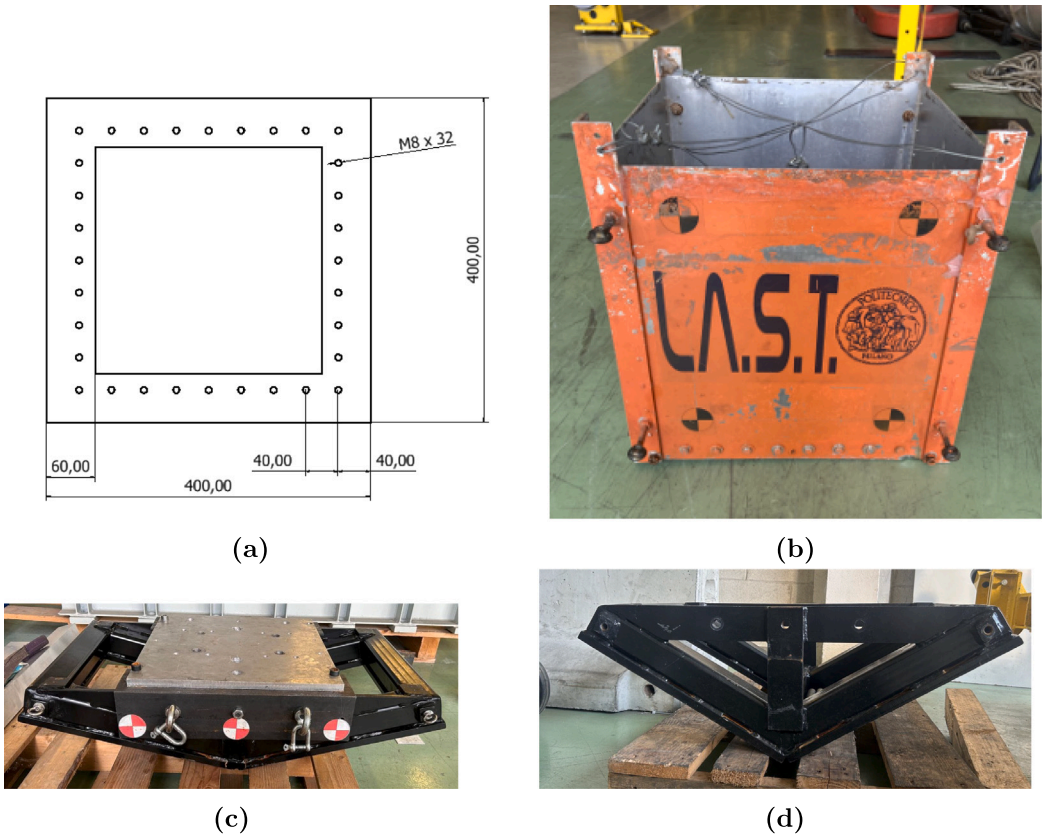

Fig. 1. Test fixtures used in the experimental campaign. (a) Fixture frame dimensions. (b) 0° test article. (c) 15° test article. (d) 30° test article.

Table 1
Summary of experimental tests performed.

Specimen	Desired impact angle [°]	Mass [kg]	Measured impact velocity $\left[\frac{m}{s}\right]$	Panel thickness [mm]	Measured impact angle [°] (frontal view)	Measured impact angle [°] (lateral view)
A1_0_m1	0	50	7.2	1.02	1.5	1
A2_0_m1	0	50	7.2	1.02	0	0.6
A3_0_m2	0	114	7.2	1.02	−0.2	0.2
A4_0_m2	0	114	7.2	1.02	1	0.3
B1_0_m2	0	114	7.2	1.6	0.2	0.2
B2_0_m2	0	114	7.2	1.6	1	0.5
A1_15_m1	15	75	7.6	1.02	14.2(left) 15.8 (right)	2
A2_15_m1	15	75	7.6	1.02	14.5(left) 15.5 (right)	2
A1_30_m1_v1	30	75	7.3	1.02	29.1(left) 30.9 (right)	0.4
A2_30_m1_v1	30	75	7.3	1.02	29.9(left) 30.1 (right)	0.3
A3_30_m1_v2	30	75	5.5	1.02	30	1
A4_30_m2_v2	30	150	5.4	1.02	30.5 (left) 29.5 (right)	1
A5_30_strain	30	75	7.4	1.02	–	–
A6_30_strain	30	75	7.4	1.02	29.5 (left) 30.5 (right)	2

however, from instabilities during large deformation, and the Eulerian one, in which the mesh is fixed and the material flows through it. Hence, this algorithm allows to reduce negative effects due to large mesh distortion for highly non-linear simulations, like fluid dynamics problems. The Eulerian method is actually a subset of the ALE method where the reference mesh remains fixed in space [21]. Computationally, the ALE algorithm comprises a first *Lagrangian step* where the solution is advanced in time with a conditionally stable, second-order accurate central difference method [46] and a second *advection step*, during which the element state variables are remapped back onto a moving reference mesh [47], following the volume variations of the element during each timestep. For the advection step, the Van Leer algorithm [48] was chosen for the computation of the transport of the element-centered variables (e.g. density, internal energy, stress tensor) being second-order accurate, monotonic and conservative [49,50]. Instead, for the momentum transport, the Half Index Shift algorithm was used [51] to inhibit dispersion errors and preserve monotonicity of the velocity field [50].

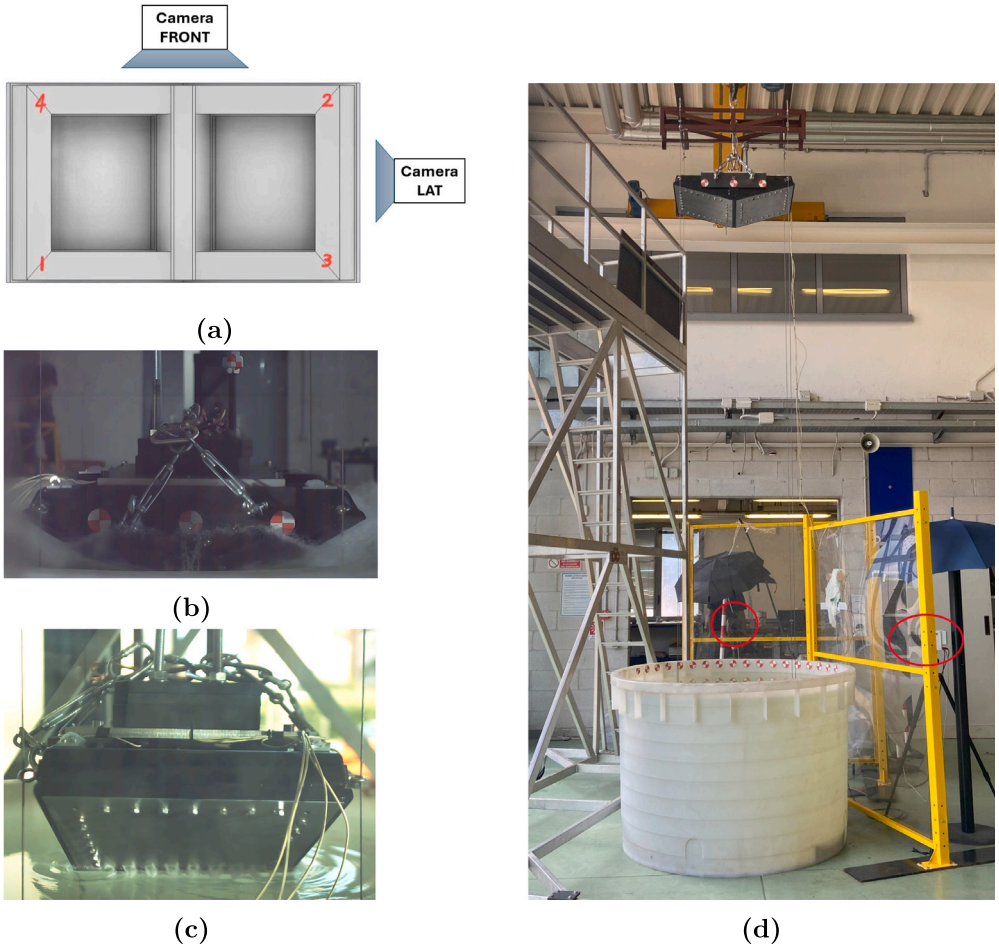

Fig. 2. Experimental setup of impact tests. (a) Schematic overview of the cameras and accelerometers positions in red. (b) Frontal view of the test. (c) Lateral view of the test. (d) Overall setup.

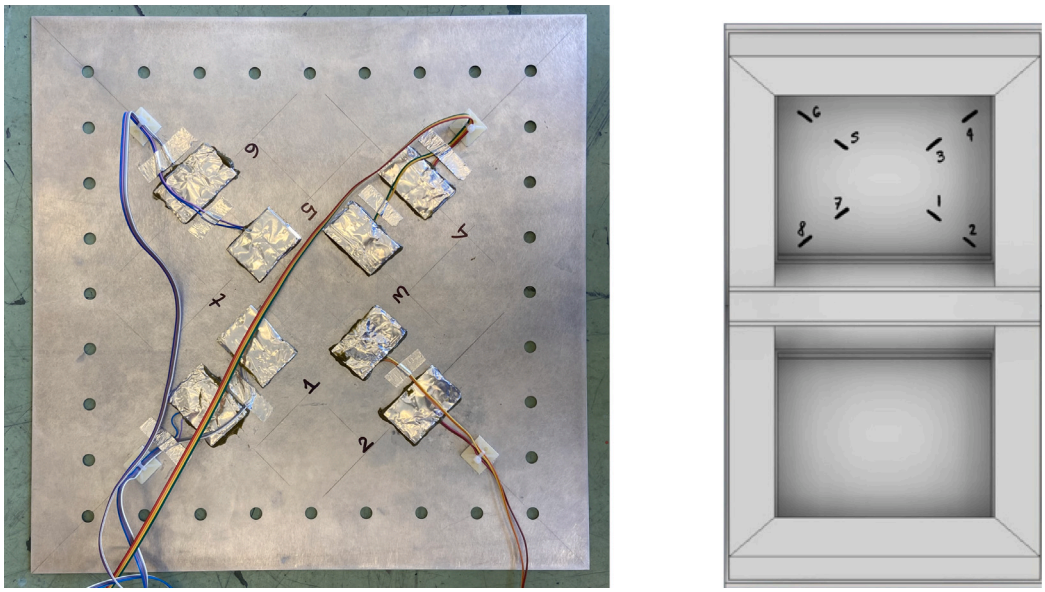

Fig. 3. Positions of the strain gauges mounted on one of the panels tested at 30°.

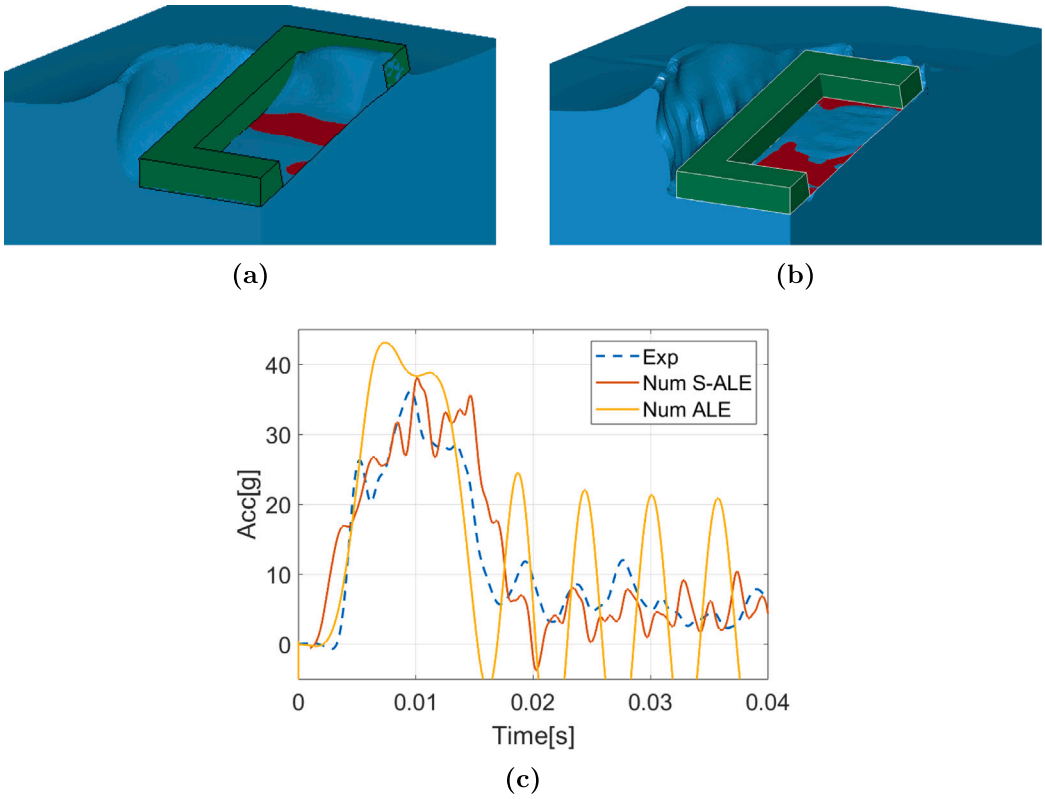

Fig. 4. Comparison between two different fluid formulations in LS-Dyna for the impact of 15° wedge (quarter section is showed), with emphasis given to the difference in leakage: (a) ALE formulation. (b) S-ALE formulation. (c) Comparison of acceleration data.

However, in the present paper, a recent version of the ALE method is used, defined in LS-DYNA as Structured ALE (S-ALE) [52,53]. The main difference lies in the fluid–structure interaction, implemented to automatically reduce *leakage*, a numerical phenomenon consisting in the undesired compenetration between the fluid part and the Lagrangian part, thanks to a energy balance control algorithm allowing better estimation of the penalty spring stretch [54]. The effect of this interaction algorithm (which translates in the software into the replacement of the keyword *CONSTRAINED_LAGRANGE_IN_SOLID with *ALE_STRUCTURED_FSI) can be clearly seen in Fig. 4, where it is shown a comparison between the two methods for the impact with 15° wedge. In particular, the ALE formulation, with the contact stiffness calibrated to fit the experimental data across all the tests performed, (Fig. 4(a)) showed in some cases so significant leakage that the water wave surpassed the inner part of the fixture (light-blue colored part), instead of flowing underneath it, resulting in massive oscillations in the acceleration measured, as illustrated in Fig. 4(c).

Both air and water parts were modeled in the simulations using a multi-material formulation in which both fluids were able to flow through ALE mesh elements and to be present at the same time inside the same element [47]. Linear polynomial laws were used based on literature studies [21] for the fluids equations of state. In Table 2 are reported the values used, following the formulation defined in Eq. (1), where P was the internal pressure, E the internal energy, and μ, set to zero at the beginning of the simulation, was defined by Eq. (2), where $\frac{\rho}{\rho_0}$ was the ratio between density at each step during simulation and reference density.

$$P = C_0 + C_1\mu + C_2\mu^2 + C_3\mu^3 + (C_4 + C_5\mu + C_6\mu^2)E \tag{1}$$

$$\mu = \frac{\rho}{\rho_0} - 1 \tag{2}$$

Table 2
Constants used for definition of fluids equations of state following linear polynomial equation (1).

Fluid	C_0 [MPa]	C_1 [MPa]	C_2 [MPa]	C_3 [MPa]	C_4 [MPa]	C_5 [MPa]	C_6 [MPa]
Air [21]	0	0	0	0	0.4	0.4	0
Water [1]	0	2723	7727	14 600	0	0	0

The aluminum plates were modeled using fully integrated shell elements and a material model with full characterization of the plastic regime, but without strain rate or temperature dependence, considered not significant for the impact conditions of interest. The plates were connected to the fixture by tied contacts with the whole surface of the square frame. Moreover, even though the fixtures used for the 0° test and for the wedged tests were different due to the manufacturing method (the first one was solid aluminum, the second one was made of steel tubes), in the numerical simulations it was always considered a solid aluminum fixture, since the cross-section of the steel tubes was chosen in order to have a comparable moment of inertia with respect to the solid aluminum one.

Penalty-based coupling was used for the interaction between the Lagrangian and the Eulerian parts. This type of contact was preferred with respect to the constraint-based one because it preserves the total kinetic energy of the system after the impact and because it was considered more versatile in the calibration of the intensity of the fluid–structure interaction. The algorithm worked by computing at each time step the penetration distance d between the Lagrangian and ALE parts in specific points of the elements (called coupling points). Then, a counteracting force was applied to both nodes of the ALE and Lagrangian parts proportionally to the penetration distance multiplied by the stiffness coefficient k, according to Eq. (3). The stiffness of the

Table 3
Comparison of full fluid-domain simulations, performed on a cluster with 32 cores and massively parallel processing (MPP), varying element sizes of the Lagrangian shell (Lagr) and of ALE Fluids.

Mesh Size			Acceleration	Residual	Computational
Lagr	ALE Fluids		Peak [g]	Internal	time [min]
[mm]	Width [mm]	Depth [mm]		Energy [J]	
8	10	10	146.4	36.8	24
6	7	7	153.8	33.1	100
6	7	4	151.9	26.9	169
5	6	6	149.5	31.4	169
4	5	5	151.8	28.9	387
3	7	4	148.6	29.6	428
3	4	4	153.2	27.3	1187

contact was computed according to Eq. (4) [49], where K_t was the bulk modulus, A_t the surface of the contact area, V_t the volume of the master element, and p_{fac} the penalty factor, a non-physical scaling multiplier of the contact stiffness that could be inserted by the user, and that in this case was calibrated based on the experimental test campaign.

$$F_{fsi} = -k\,d \tag{3}$$

$$k = p_{fac}\,\frac{K_t\,A_t^2}{V_t} \tag{4}$$

The element dimensions were chosen as a result of a sensitivity analysis performed with the case of the 0° impact and full fluid domain modeling, looking at the most effective balance between accuracy and computational time, summarized in Fig. 5 and Table 3. Since these sensitivity studies were conducted preliminarily with respect to the FSI penalty factor calibration, which will be described subsequently, the default suggested constant value of p_{fac} 0.1 was used [47]. The relative size between Lagrangian shell elements and Eulerian elements at the contact surface interface was always kept around a 1.2 ratio, default suggested value of LS-DYNA Aerospace Working Group for interactions between ALE and Lagrangian elements [55]. The minimum element size considered was of 3 mm for the Lagrangian shells and 4 mm for the ALE hexahedral elements, increasing progressively up to 8 mm for the Lagrangian and 10 mm for the ALE elements. In this context, the main evaluation metrics were the acceleration response and the internal energy of the plate elements during the impact, which could be directly correlated to the amount of elastic and plastic deformation due to the water impact event. However, it was noticed that a good modeling strategy consisted in decreasing the element size of the ALE elements in the vertical direction, which was the main direction of penetration in water, while keeping the suggested mesh ratio in the other directions. Therefore, after these evaluations, we opted to use in all the simulations the mesh size of 6 mm for the Lagrangian shell elements and 7 mm wide, 4 mm deep for the ALE elements.

Another condition that the fluid mesh needed to fulfill was that the total dimensions of the fluid domain should have been sufficient not to interfere excessively with fluid dynamics, at least for the time span of interest to the first acceleration peak response. As suggested by previous studies, the dimensions of the fluid domain were set in order to be twice bigger than the dimensions of the impacting object [1,21]. In the case of 15° and 30° impacts, these constraints already matched the experimental setup in the larger dimension, for which no flow boundary was used. In the remaining test cases, it was verified that there was a negligible difference versus numerical simulation of the actual pool size used in the experimental tests, and non-reflecting boundary conditions were used in order to avoid interference with the wave propagated by the impact (which, at the speed of sound in water, $c = 1481\ \frac{\mathrm{m}}{\mathrm{s}}$, would have traveled back the smaller dimension of the numerical pool, $l = 400$ mm, in only 0.5 ms). In the vertical dimension, the depth of the pool was decreased progressively, starting from the actual depth used in the experimental tests (1000 mm), and it was found that up to a depth of 600 mm the acceleration response was not significantly affected for the time span of the first acceleration peak. These approximations however, did not allow a precise comparison of the water level difference after the impacts between numerical and experimental results. For each simulation, two symmetry conditions were enforced to decrease the computational time.

Regarding the calibration of the FSI properties, once defined the optimal mesh properties, the choice of the optimal penalty factor was driven by a trade-off between correlation with experimental tests, numerical noise (which increased with softer contact stiffness) and *leakage*. This last phenomenon is an adverse but unavoidable consequence of the penalty coupling method. However, it should be kept to the minimum possible in order to prevent non-physical behaviors of the fluid and undesired interference with parts of the structure not in contact with the fluid. In the simulations, the leakage was quantified based on the contour plots, considering the maximum compenetration between the water level and the plate surface mesh at the center of the panel, which is the most critical point, using as benchmark the test A1_0_m1 (0°, M = 50 kg, $v = 7.2\ \frac{\mathrm{m}}{\mathrm{s}}$).

In LS-DYNA, the penalty factor can be either a constant value or can be defined by a curve, which depends on the penetration distance. In this regard, several analyses were conducted on fluid–structure interaction with water using different penalty factors in order to find the most suitable one for the correlation with experimental tests, both using constant values and linear laws (summarized in Table 4 and Fig. 6). It can be noticed that in order to get close to the acceleration peak of the experimental results, the constant value of penalty factor needed to be greatly decreased with respect to the recommended one [47], with a strong nonlinear influence on leakage and acceleration peak values (see Figs. 7 and 8). Instead, as also established in previous work [56], changing the slope of a linear penalty factor curve was found to give more consistent and predictable results. This was actually true for the correlation with the 0° tests, but the influence of different penalty factors values was negligible instead on wedged 15° and 30° results. The critical role of the 0° test in the calibration of the contact stiffness and leakage evaluation was probably due, in this case, to the abrupt change of contact surface in a small timestep, leading to a fast redistribution of the stresses. With the purpose of choosing the best fitting penalty factor curve with the experimental tests using objective and quantitative comparison criteria, different comparison metrics were taken into account, as defined in the recommended procedures for verification and validation of computer simulations, originally developed for roadside safety applications (RSVVP) [57]. In Fig. 9 the most significant numerical simulation curves are compared to the experimental one for the test performed at 0 degree, M = 50 kg, $v = 7.2\ \frac{\mathrm{m}}{\mathrm{s}}$. Sprague-Geers and Knowle-Gear validation metrics were considered. Both are magnitude-phase-comprehensive (MPC) methods, where the errors on magnitude (M) and phase (P) of the curves are treated separately, and then combined with specific weights in a comprehensive (C) metric. They were selected since they allowed for systematic comparison of signals over time, being robust and only marginally influenced by the noise of highly dynamic transient signals occurring during impact events, such as ditching tests. The second one differs slightly from other MPC-type metrics since it is based on a point-to-point comparison and requires that the two curves to be compared are first synchronized in time based on the so-called time of arrival (TOA), which represents the time at which a curve reaches 5% of the peak value [57,58]. Specific formulas for such comparison metrics can be found in literature [57]. For completeness, also the ANOVA method was used, computing the average residual error and the standard deviation of the residual error resulting from a point-to-point comparison of the numerical and experimental curves. Looking at the different curves, the *mod6* was selected, since it showed consistent best results for all Knowle-Gear metrics and second best results for all Sprague-Geers metric, with good correlation also for the ANOVA metrics.

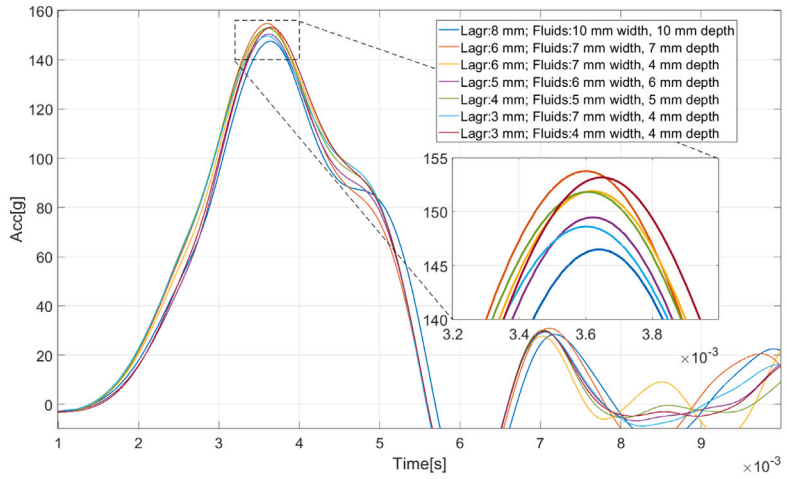

(a)

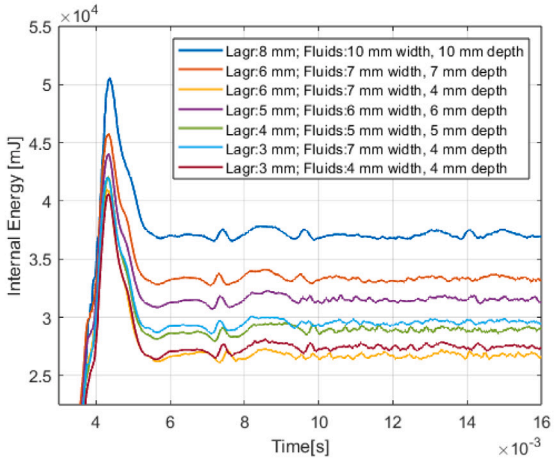

(b)

Fig. 5. Sensitivity study for water impact of 0° fixture, changing element size (first number indicates the dimension of the Lagrangian shell, followed by ALE element size in the width and depth directions). (a) Acceleration force response comparison, with zoom on acceleration peak comparison. (b) Panel internal energy comparison.

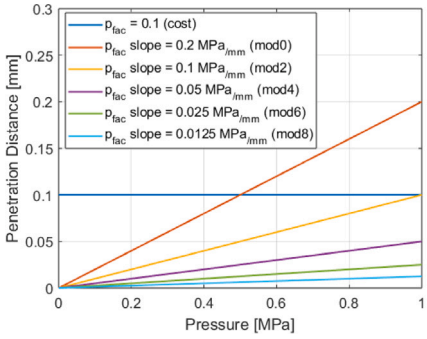

Fig. 6. Summary of penalty factor laws tested (0°, M = 50 kg, v = 7.2 $\frac{m}{s}$).

The analyses performed at different penalty factors were conducted with interaction only between Lagrangian parts and water ALE domain. However, when evaluating the results with this setup in the post-processing phase, it was noticed that, after the first springback motion of the aluminum plate during the impact, a large air pocket originated

Table 4
Maximum leakage values for the different penalty factors tested (0°, M = 50 kg, v = 7.2 $\frac{m}{s}$).

Name	P_{fac} slope [$\frac{MPa}{mm}$]	P_{fac} const values	Leakage [mm]
cost	–	0.1	0
cost2	–	0.2	0
cost3	–	0.05	0
cost4	–	0.01	0
cost5	–	0.001	1
cost6	–	10^{-4}	21
cost7	–	$5 * 10^{-5}$	22
cost8	–	$2 * 10^{-5}$	25
mod0	0.2	–	13
mod2	0.1	–	14
mod4	0.05	–	15
mod6	0.025	–	21
mod8	0.0125	–	30

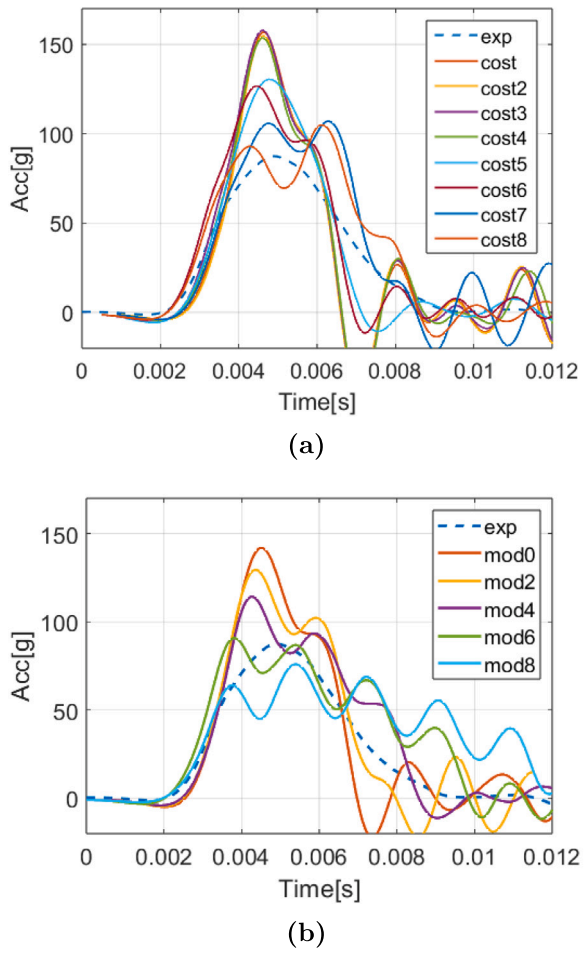

Fig. 7. Summary of sensitivity studies performed on the penalty factor in comparison with experimental data. Influence on accelerometers results for test A1_0_m1 (0°, M = 50 kg, v = 7.2 $\frac{m}{s}$). (a) Constant penalty factors values (cost = 0.1, cost2 = 0.2, cost3 = 0.05, cost4 = 0.01, cost5 = 0.001, cost6 = 10^{-4}, cost7 = $5 * 10^{-5}$, cost8 = $2 * 10^{-5}$) (b) Penalty factors linearly variable with penetration distance (with slope = 0.2 MPa/mm for mod0, slope = 0.1 MPa/mm for mod2, slope = 0.05 MPa/mm for mod4, slope 0.025 MPa/mm for mod6, slope = 0.0125 MPa/mm for mod8).

underneath the plate. This phenomenon reduces the panel's adhesion to the water, limiting the effectiveness and duration of the fluid–structure interaction. The solution found to this non-physical water behavior was to add a second fluid–structure interaction, defined with a different input card, between the Lagrangian parts and the air ALE part. After several attempts, it was still used a linear penalty factor curve, but with the slope ten times less than the one used for contact with water, in order to limit the interference with it. In Fig. 10 it can be seen the improved water behavior, which now maintained contact with shell elements always throughout the simulations. The correctness of the behavior was also indicated by water starting to flow over the solid aluminum fixture after the impact (the simulation was, in fact, simplified with respect to the reality where at the border of the fixture there were four vertical walls, but the effect of the correct mass distribution was considered).

3. Results

3.1. Experimental tests campaign

The experimental tests setup allowed to achieve a high level of repeatability, in view of the low scattering of both measures of multiple accelerometers used during the same test (Figs. 12(a), 13(a), 14(a)) and of measures of the same accelerometers in different tests performed under the same conditions (Figs. 12(b), 13(b), 14(b)). Overall, the high-speed cameras proved good balancing of the test articles at the instant of impact with water, with misalignment of max 2°, but in most of the cases of less than 1° (as reported in Table 1). Fig. 11 illustrates visually the symmetry of the impacts at water entry.

3.2. Numerical correlations

In this section, the comparison between the experimental data, presented in Section 3.1, and numerical simulations, performed with the model illustrated in Section 2.2, is reported.

With the calibrated penalty factor curves, a good correlation was found concerning the tests at 0°, also varying the mass and the thickness of the panel, as illustrated in Fig. 15. A relevant amount of oscillation was observed in the numerical acceleration plot; however, this was deemed not avoidable due to a small amount of leakage introduced as an undesired effect of the penalty factor correction, which was necessary to achieve correlation with the acceleration peak, as already reported in Section 2.2. The wedged impact showed good correlation between the numerical model and the experimental tests, as illustrated in Figs. 16 and 17. In these cases, being the influence of the calibrated penalty factor curve lower, the consistency of the results supported the overall accuracy of the S-ALE method used. Notably, also the strain gauges did correlate precisely with the numerical simulations (Fig. 18), looking at the strains in the element closest to the actual position of the sensors in the test. Strain measures were compatible with the out-of-plane bending of the plate, with fixed boundary conditions on the framed extremities, showing higher values closer to the center of the panel (strain gauges 1, 3, 5, 7).

4. Discussion

4.1. Highlights of the study

The article features a uniquely comprehensive collection of experimental data correlated with numerical simulations of water impacts of thin aluminum panels compatible with those used for helicopter fuselages in a wide range of impacting angles, ballast masses and velocities.

The accuracy of the test setup allowed us to obtain repeatable results and to study the influence of panel deformability in ditching conditions, featuring also, in some cases, the use and validation of strain gauges together with the accelerometers. In fact, measuring strain histories in the 30° test gave additional information on local stress distribution on the panels during impact. Interestingly, it was possible to observe a first initial peak, progressing in time with the spray root position along the wedge. Subsequently, locally, a plateau deformation value, corresponding to residual water pressure loads after first impulsive phase, was noticed. In the final stage, strain measures oscillated around null values after the impact phase, suggesting the absence of plastic deformation.

The assessment of the influence of panel flexibility is particularly relevant for the outcome of ditching events, since it may alter the load and stress distribution on the structure, the accelerations on the occupants, and, ultimately, the buoyancy of the fuselage [59]. Previous literature studies highlighted the importance of considering high-intensity impacts in order to capture the 'hydroplastic' effects of the event [60]. Most of the times, these effects are investigated in case studies of full-scale models [12,61], more rarely in more controllable smaller setups [62,63]. In the present experimental campaign, the panels impacting water at 0° experienced plastic deformation as a result of the water slamming. Moreover, further underlining the importance of studying the deformability of the panels, it was noticed, comparing impacts at same inclination angle of 0°, same velocity and mass, but

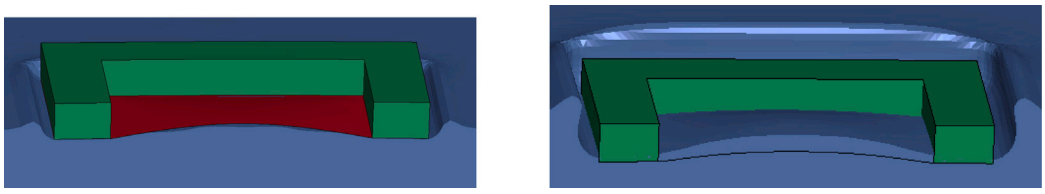

(a) (b)

Fig. 8. Comparison of leakage between numerical simulations with two different p_{fac} curves (0°, M = 50 kg, v = 7.2 $\frac{m}{s}$). (a) p_{fac} cost (0.1) (b) p_{fac} mod6.

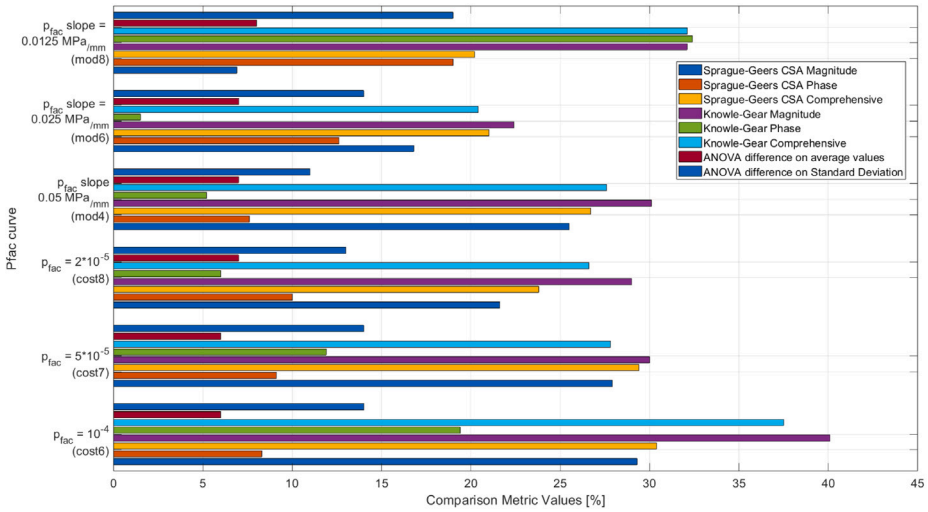

Fig. 9. RSVVP comparison metrics for best performing pfac curves with respect to experimental acceleration curve of test A1_0_m1 (0°, M = 50 kg, v = 7.2 $\frac{m}{s}$) (Lower is better).

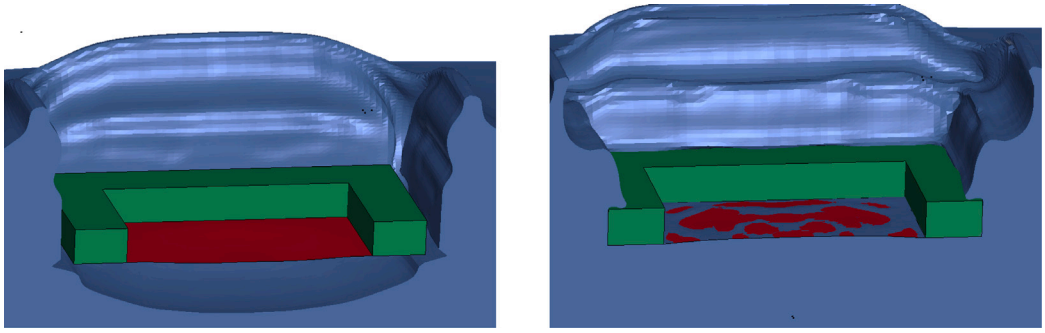

(a) (b)

Fig. 10. Comparison between different water ALE behaviors with emphasis on the post-springback behavior. (a) FSI only with water. (b) FSI with both water and air.

different thickness of the panels, that the acceleration peak increased with the thickness of the panel. Interestingly, the influence of panel stiffness on measured water loads was supported by previous literature studies [32,33]. *Iafrati et al.* observed instead an opposite trend [20], which may be related to the influence of forward velocity trapping fluid in the deformed plates.

The main purpose of our experimental campaign was to provide enough data to correlate with a comprehensive explicit FE numerical model, able to extend the database of water impact events with further configurations without the need to actually perform heavily time- and resource-consuming experimental tests. The proposed FE numerical model exploiting S-ALE formulation, which differentiates from standard methods used for ditching applications by automatically minimizing the leakage, after rigorous mesh sensitivity and parameter calibration studies, showed a satisfactory correlation with most of the experimental data at different impacting angles. Higher accuracy was achieved in the wedged 15° and 30° impacts, in the latter case also predicting strain gauge data.

The magnitude of the acceleration peaks of tests performed at 0° required a strong correction of the penalty factors with respect to default values [47]. This adjustment significantly influenced the leakage and the numerical noise of the simulation results. Nevertheless, they were deemed acceptable with respect to the primary aim of the study, achieving an accurate prediction of load distribution and of structure response to ditching. Notably, in this context, objective quantitative comparison methods, previously developed for automotive crash tests [57], were applied for the first time to ditching scenarios to determine the most accurate FSI penalty factor curve to be used in the numerical model. In fact, previous studies, correlating a numerical ALE model in LS-Dyna with experimental water impact tests, used the

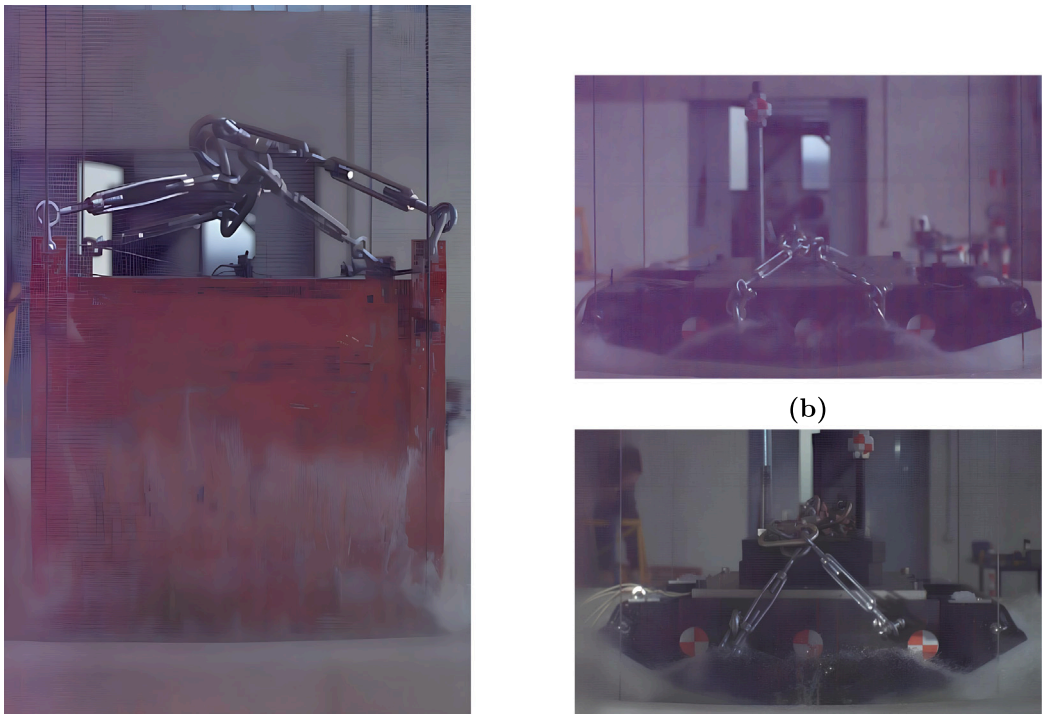

Fig. 11. Pictures from high-speed camera recording water impacts from the different experimental tests. (a) Frame from test A3_0_m2, t = 8.1 ms after water entry. (b) Frame from test A2_15_m1, t = 6.6 ms after water entry. (c) Frame from test A4_30_m2_v2, t = 18.1 ms after water entry.

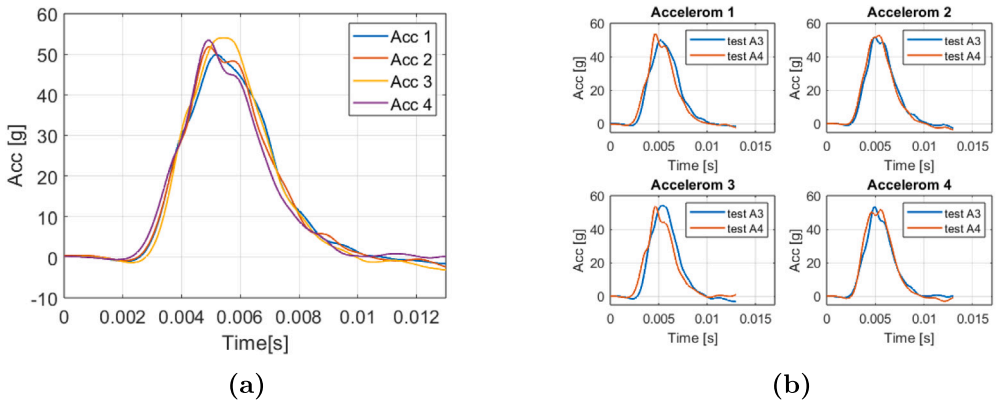

Fig. 12. (a) Accelerometers data of test A3_0_m2 (0°, M = 114 kg, v = 7.2 $\frac{m}{s}$). (b) Comparison with data from same accelerometers in test performed at same initial conditions (A4_0_m2). Accelerometers positioned as in Fig. 2(a).

default constant values to model the fluid–structure interaction, likely since wedged impacts were considered [35,64,65], which we observed to be the ones less affected by penalty factor variations. Referring to the work of Sun et al. [39], instead, while the slamming angle was null and the dimensions of the test article were larger than ours, the flexibility of the panel was much lower due to the welded stiffeners. In general, the penalty factor was already shown to be highly dependent on the specific application studied, and the use of a linear curve was already suggested and used previously [55]. Importantly, in this case, it was tuned to capture precisely acceleration data obtained at a large range of impacting angles.

The correlation reached by the numerical model with experimental data supports its applicability for the evaluation of ditching loads on more complex aeronautical structures and for the creation of a large database of water impacts of panels in a large variety of impact conditions. Ultimately, the methodology could be used for rapidly assessing ditching behavior of entire fuselages, leading to saving costs and time in aircraft design. The investigation of fluid–structure interaction in these kind of tests has high value for ditching applications, considering also previous publications on the topic, analyzing experimental and numerical behavior of free-fall vertical impacts of framed structures [66–69].

4.2. Limitations of the study

Differently from some literature experimental campaigns [20,39], no pressure sensors were used in our experimental tests. The positioning of pressure sensors on thin aluminum panels would have required pass-through holes, introducing local unwanted effects in the deformation of the panels and requiring also numerical modeling of these artificial defects created in the panels. In addition, in a highly-dynamic crashworthiness event, pressure sensors could be influenced by local effects more than acceleration sensors, generally mounted on

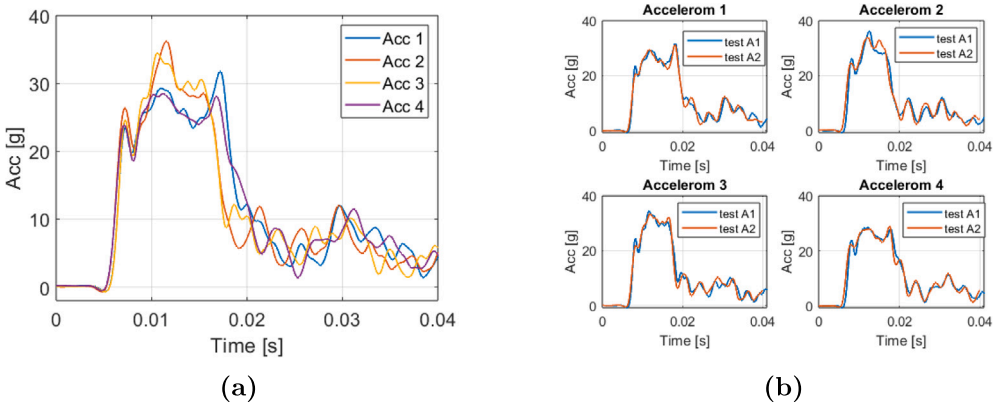

Fig. 13. (a) Accelerometers data of test A1_15_m1 (15°, M = 75 kg, v = 7.6 $\frac{m}{s}$). (b) Comparison with data from same accelerometers in test performed at same initial conditions (A2_15_m1). Accelerometers positioned as in Fig. 2(a).

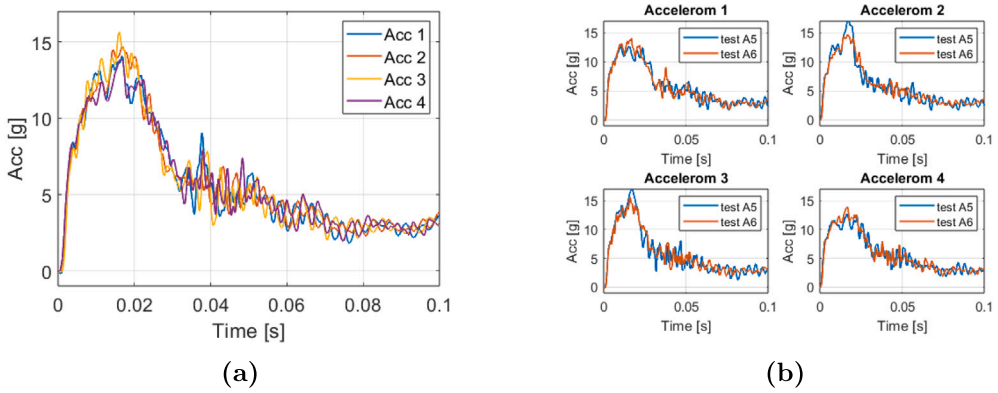

Fig. 14. (a) Accelerometers data of test A6_30_strain (30°, M = 75 kg, v = 7.4 $\frac{m}{s}$). (b) Comparison with data from same accelerometers in test performed at same initial conditions (A5_30_strain). Accelerometers positioned as in Fig. 2(a).

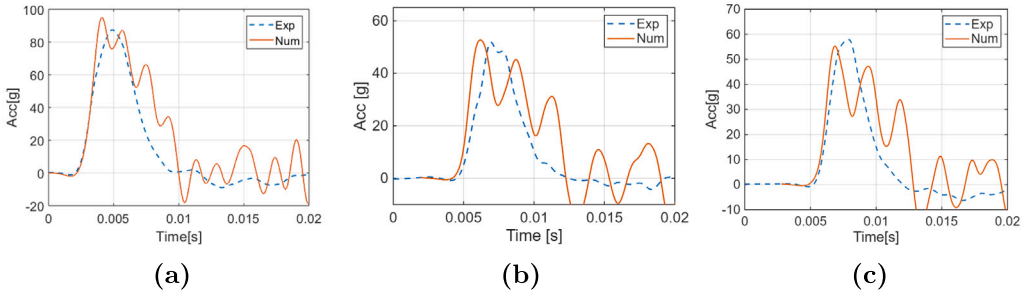

Fig. 15. Comparison of experimental and numerical acceleration data for tests performed at 0°. (a) M = 50 kg, v = 7.2 $\frac{m}{s}$, t = 1.02 mm. (b) M = 114 kg, v = 7.2 $\frac{m}{s}$, t = 1.02 mm. (c) M = 114 kg, v = 7.2 $\frac{m}{s}$, t = 1.6 mm.

stiffer parts of the structure. Our measures of acceleration and strain were considered sufficient to correlate the numerical model.

Moreover, even if the range of vertical impact velocities investigated in the experimental tests was higher with respect to the vertical sinking velocity required for ditching certification (1.5 m/s), stated in CS 29.563 for large rotorcrafts [70], it was needed to reach high impact energies in order to study hydroelastic and hydroplastic effects, given the constraints of the setup concerning dimensions of the panels and water basin. In addition, the impact severity to be evaluated during certification is highly dependent on the sea state considered and the velocity relative to the water surface may reach values close to the ones tested in our experimental campaign. It has been also suggested in literature the need for the investigation of 'controlled' ditching in aeronautical certifications, as a method to bridge the gap between 'planned' and 'unplanned' events, which would include a larger envelope of emergency landings on water, more representative of the statistics of water impact scenarios [71] and compatible with the range of impact velocities tested.

Another limitation of the study, due however to experimental setup constraints, is the lack of investigation of forward velocity in the water impacts, causing cavitation effects [5,9,20]. In this regard, helicopter ditching may be a suitable scenario, with limited forward velocity, also considering the influence of sea state, which may decrease equivalent entry angle [70]. Further work is required to evaluate the accuracy of the proposed numerical model under scenarios involving forward velocity. However, the inclusion of both air and water in the simulation model already represents an important step toward accurately

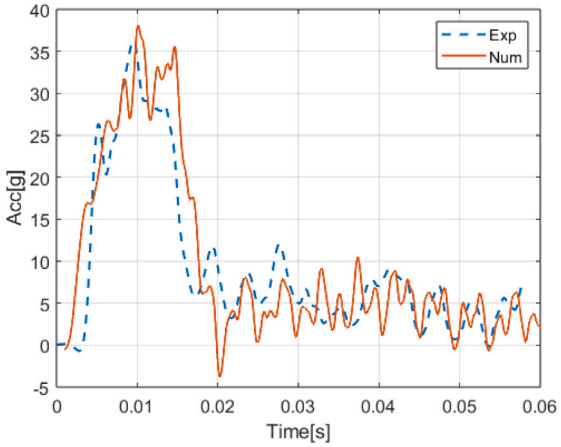

Fig. 16. Comparison of experimental and numerical acceleration data for test performed at 15°, M = 75 kg, v = 7.6 $\frac{m}{s}$.

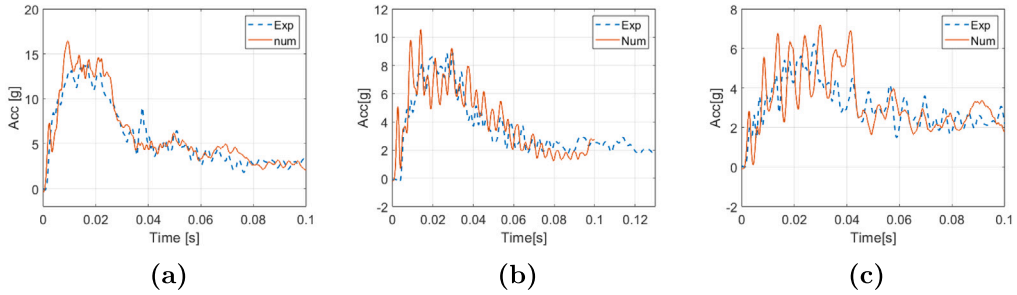

Fig. 17. Comparison of experimental and numerical acceleration data for tests performed at 30°. (a) M = 75 kg, v = 7.3 $\frac{m}{s}$. (b) M = 75 kg, v = 5.4 $\frac{m}{s}$. (c) M = 150 kg, v = 5.4 $\frac{m}{s}$.

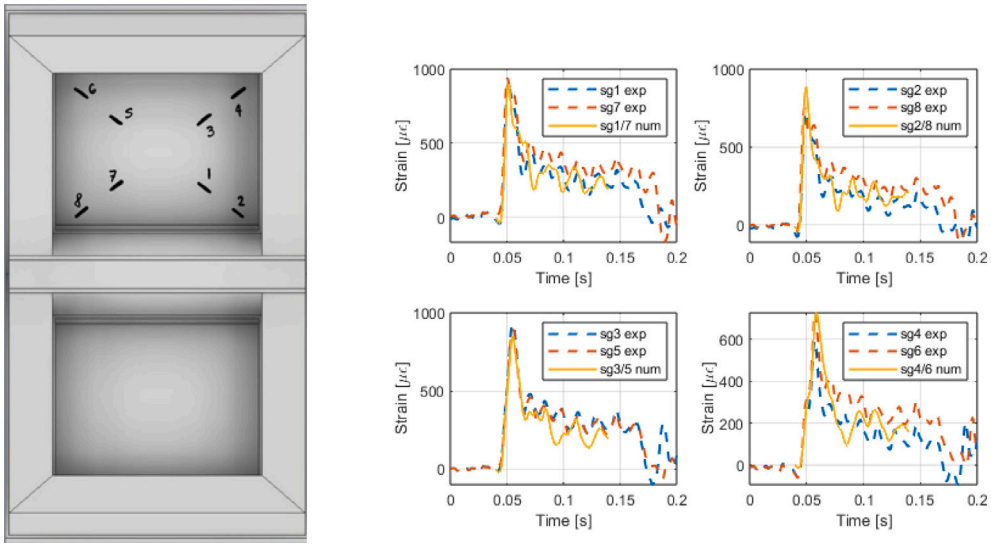

Fig. 18. Comparison of experimental and numerical strain gauge data (sg) for tests performed at 30°, M = 75 kg, v = 7.4 $\frac{m}{s}$.

capturing water cavitation and air entrapment effects. Other areas of interest for future research may include the interaction between different panels in a complete deformable aeronautical structure, the impact resistance of emergency flotation systems and of novel energy-absorption systems [72,73], in order to obtain a more comprehensive evaluation and analysis of ditching events.

5. Conclusions

In conclusion, we developed a numerical model for vertical water impacts using S-ALE approach which accurately correlated with experimental acceleration and strain gauge data across different impact angles, masses and velocities tested. Quantitative methods previously

used for roadside safety applications were for the first time used in ditching scenarios to compare numerical and experimental acceleration curves, obtaining the model with the best fitting penalty factor curves.

The numerical model can be used to reliably explore a wide range of ditching configurations and to extend investigations to aeronautical structures of varying complexity, up to full-scale subfloors or fuselages. This approach enables the creation of a comprehensive dataset that can support the development of simplified, data-driven numerical tools capable of efficiently estimating ditching scenarios, useful to significantly reduce computational time and to be effectively integrated into the early design stages of novel aircraft models.

CRediT authorship contribution statement

Alessandro Giustina: Writing – review & editing, Writing – original draft, Visualization, Validation, Software, Methodology, Investigation, Formal analysis, Data curation. **Ivan Colamartino:** Writing – review & editing, Validation, Formal analysis. **Stefano Dolci:** Writing – review & editing, Methodology. **Marco Anghileri:** Writing – review & editing, Supervision, Conceptualization.

Declaration of competing interest

The authors declare that they have no known competing financial interests or personal relationships that could have appeared to influence the work reported in this paper.

Acknowledgment

This work was supported by European Union - Next Generation EU, Mission 4, Component 1, CUP D43C23002190008.

Data availability

Data will be made available on request.

References

[1] Toso N. Contribution to the modelling and simulation of aircraft structures impacting on water. (Ph.D. diss.), Universitat Stuttgart; 2009, URL https://api.semanticscholar.org/CorpusID:106667368.

[2] Brooks CJ, MacDonald CV, Baker SP, Shanahan DF, Haaland WL. Helicopter crashes into water: warning time, final position and other factors affecting survival. Aviat Space Environ Med 2014;85(4):440–4. http://dx.doi.org/10.3357/asem.3478.2014.

[3] Schick VC, Boyd DD, Hippler C, Hinkelbein J. Survival after ditching in motorized aircraft, 1989 - 2022. Aerosp Med Hum Perform 2024;95(5):254–8. http://dx.doi.org/10.3357/AMHP.6332.2024.

[4] Aziz A, Sariff ESM, Shamsudheen I, Abd Jamil R, Zarim MAUAA. The effect of emergency floatation system (EFS) on helicopter stability during ditching. Transp Eng 2023;14:100206. http://dx.doi.org/10.1016/j.treng.2023.100206.

[5] SARAH Consortium. Increased safety & robust certification for ditching of aircrafts & helicopters, D2.3: Final progress report. 2020, URL https://cordis.europa.eu/project/id/724139/results.

[6] Spinosa E, Broglia R, Iafrati A. Hydrodynamic analysis of the water landing phase of aircraft fuselages at constant speed and fixed attitude. Aerosp Sci Technol 2022;130:107846. http://dx.doi.org/10.1016/j.ast.2022.107846.

[7] Luo W, Gu W, Huang Y, Chang L. Experimental investigation of dynamic characteristic during civil aircraft ditching. Chin J Aeronaut 2025;38(4):103281. http://dx.doi.org/10.1016/j.cja.2024.10.013.

[8] Climent H, Benitez L, Rosich F, Rueda F, Pentecote N. Aircraft ditching numerical simulation. In: 25th international congress of the aeronautical sciences. 2006, URL https://icas.org/icas_archive/ICAS2006/PAPERS/268.PDF.

[9] Iafrati A, Grizzi S, Siemann M, Benítez Montañés L. High-speed ditching of a flat plate: Experimental data and uncertainty assessment. J Fluids Struct 2015;55:501–25. http://dx.doi.org/10.1016/j.jfluidstructs.2015.03.019.

[10] Siemann MH, Schwinn DB, Scherer J, Kohlgrüber D. Advances in numerical ditching simulation of flexible aircraft models. Int J Crashworthiness 2018;23(2):236–51. http://dx.doi.org/10.1080/13588265.2017.1359462.

[11] Spinosa E, Grizzi S, Iafrati A. High-speed ditching of double curvature specimens with cavitation and ventilation. Ocean Eng 2025;341:122209. http://dx.doi.org/10.1016/j.oceaneng.2025.122209.

[12] Pentecôte N, Vigliotti A. Crashworthiness of helicopters on water:Test and simulation of a full-scale WG30 impacting on water. Int J Crashworthiness 2003;8:559–72. http://dx.doi.org/10.1533/cras.8.6.559.19259.

[13] Wittlin G, Schultz M, Smith MR. Rotary wing aircraft water impact test and analyses correlation. In: Presented at the American Helicopter Society 56 Annual Forum, Virginia Beach, Virginia, May 2-4, 2000. URL https://www.mscsoftware.co.kr/upfile/pro_pdf/200_Helicopter_Water_Impact.pdf.

[14] Goodwin JF. DC-10 airplane: Design ditchability, structural aspects. In: Pacific Air Safety Research and Rescue Symposium. 1968, p. 19–23.

[15] Zheng Y, Qu Q, Liu P, Shi X, Zhou P. Ditching performance comparison of blended-wing-body and tube-and-wing aircraft. J Aircr 2025;1–14. http://dx.doi.org/10.2514/1.C038372.

[16] Pellettiere JA. Expanded use of modeling and simulation in ditching applications. Technical report DOT/FAA/AM25/06, 2025, URL https://rosap.ntl.bts.gov/view/dot/82313.

[17] Guo B, Liu P, Qu Q, Wang J. Effect of pitch angle on initial stage of a transport airplane ditching. Chin J Aeronaut 2013;26(1):17–26. http://dx.doi.org/10.1016/j.cja.2012.12.024.

[18] Ding S, Liu P, Wen X, Qu Q. Numerical study of skipping motion of blended-wing-body aircraft ditching on calm/wavy water. J Aircr 2024;61(6):1700–16. http://dx.doi.org/10.2514/1.C037721.

[19] Lu Y, Buono AD, Xiao T, Iafrati A, Deng S, Xu J. On applicability of von karman's momentum theory in predicting the water entry load of V-shaped structures with varying initial velocity. Ocean Eng 2022;262:112249. http://dx.doi.org/10.1016/j.oceaneng.2022.112249.

[20] Iafrati A, Grizzi S, Olivieri F. Experimental investigation of fluid–structure interaction phenomena during aircraft ditching. AIAA J 2021;59(5):1561–74. http://dx.doi.org/10.2514/1.J059458.

[21] Bisagni C, Pigazzini M. Modelling strategies for numerical simulation of aircraft ditching. Int J Crashworthiness 2018;23(4):377–94. http://dx.doi.org/10.1080/13588265.2017.1328957.

[22] Anghileri M, Castelletti LML, Francesconi E, Milanese A, Pittofrati M. Survey of numerical approaches to analyse the behavior of a composite skin panel during a water impact. Int J Impact Eng 2014;63:43–51. http://dx.doi.org/10.1016/j.ijimpeng.2013.08.008.

[23] Xiao T, Qin N, Lu Z, Sun X, Tong M, Wang Z. Development of a smoothed particle hydrodynamics method and its application to aircraft ditching simulations. Aerosp Sci Technol 2017;66:28–43. http://dx.doi.org/10.1016/j.ast.2017.02.022.

[24] Groenenboom PHL, Campbell J, Benitez Montanes L, Siemann M. Innovative SPH methods for aircraft ditching. In: 11th world congress on computational mechanics. 2014, URL https://congress.cimne.com/iacm-eccomas2014/admin/files/filePaper/p2984.pdf.

[25] Vacondio R, Altomare C, De Leffe M, Hu X, Le Touzé D, Lind S, Marongiu JC, Marrone S, Rogers BD, Souto-Iglesias A. Grand challenges for smoothed particle hydrodynamics numerical schemes. Comput Part Mech 2020;8:575–88. http://dx.doi.org/10.1007/s40571-020-00354-1.

[26] Siemann M, Langrand B. Coupled fluid-structure computational methods for aircraft ditching simulations: Comparison of ALE-FE and SPH-FE approaches. Comput Struct 2017;188:95–108. http://dx.doi.org/10.1016/j.compstruc.2017.04.004.

[27] Leon Muñoz C, Kohlgrüber D, Langrand B. Analysis of the application of fuselage skin reinforcements with beam element representations in flexible full aircraft models for ditching simulations. IOP Conf Ser: Mater Sci Eng 2022;1226(1):012057. http://dx.doi.org/10.1088/1757-899X/1226/1/012057.

[28] Jackson KE, Putnam JB. LS-DYNA®Water Ditching simulation of a Fokker F28 Fellowship Aircraft. NASA/TM–2020-5006941, 2020, URL https://ntrs.nasa.gov/api/citations/20205006941/downloads/NASA-TM-2020-5006941.pdf.

[29] Tveitnes T, Fairlie-Clarke AC, Varyani K. An experimental investigation into the constant velocity water entry of wedge-shaped sections. Ocean Eng 2008;35(14):1463–78. http://dx.doi.org/10.1016/j.oceaneng.2008.06.012.

[30] Tenzer M, el Moctar O, Schellin TE. Experimental investigation of impact loads during water entry. Ship Technol Res 2015;62(1):47–59. http://dx.doi.org/10.1179/0937725515Z.0000000003.

[31] Ren Z, Javaherian MJ, Gilbert CM. Kinematic and inertial hydroelastic effects caused by vertical slamming of a flexible V-shaped wedge. J Fluids Struct 2021;103:103257. http://dx.doi.org/10.1016/j.jfluidstructs.2021.103257.

[32] Tödter S, El Moctar O, Neugebauer J, Schellin TE. Experimentally measured hydroelastic effects on impact-induced loads during flat water entry and related uncertainties. J Offshore Mech Arct Eng 2020;142(1):011604. http://dx.doi.org/10.1115/1.4044632.

[33] Hosseinzadeh S, Tabri K, Hirdaris S, Sahk T. Slamming loads and responses on a non-prismatic stiffened aluminium wedge: Part I. Experimental study. Ocean Eng 2023;279:114510. http://dx.doi.org/10.1016/j.oceaneng.2023.114510.

[34] Meziane B, Alaoui AEM, Nême A, Leble B, Bellanger D. Experimental investigation of the influence of the panel stiffness on the behaviour of a wedge under slamming. J Fluids Struct 2022;114:103702. http://dx.doi.org/10.1016/j.jfluidstructs.2022.103702.

[35] Luo H, Wang H, Guedes Soares C. Numerical and experimental study of hydrodynamic impact and elastic response of one free-drop wedge with stiffened panels. Ocean Eng 2012;40:1–14. http://dx.doi.org/10.1016/j.oceaneng.2011.11.004.

[36] Luo H, Zhao Z, Xie P, Wu H, Li X. Experimental and numerical investigation on hydroelastic impact of one free-drop wedge with aluminum stiffened panels. In: OCEANS 2014-taipei. IEEE; 2014, p. 1–7. http://dx.doi.org/10.1109/OCEANS-TAIPEI.2014.6964307.
[37] Shams A, Zhao S, Porfiri M. Hydroelastic slamming of flexible wedges: Modeling and experiments from water entry to exit. Phys Fluids 2017;29(3). http://dx.doi.org/10.1063/1.4978631.
[38] Hassoon OH, Tarfaoui M, Alaoui AEM. An experimental investigation on dynamic response of composite panels subjected to hydroelastic impact loading at constant velocities. Eng Struct 2017;153:180–90. http://dx.doi.org/10.1016/j.engstruct.2017.10.029.
[39] Sun H, Y. WD. Experimental and numerical analysis of hydrodynamic impact on stiffened side of three-dimensional elastic stiffened plates. Adv Mech Eng 2018;10(4):1687814018767705. http://dx.doi.org/10.1177/1687814018767705.
[40] Dong C, Sun S, Song H, Wang Q. Numerical and experimental study on the impact between a free falling wedge and water. Int J Nav Archit Ocean Eng 2019;11(1):233–43. http://dx.doi.org/10.1016/j.ijnaoe.2018.04.004.
[41] Leon Muñoz C, Kohlgrüber D, Petsch M. High-fidelity aircraft simulations for the application in an industrialized ditching analysis process. AIAA J 2025;63(8):3487–92. http://dx.doi.org/10.2514/1.J065220.
[42] Leon Muñoz C, Petsch M, Kohlgrüber D, Pedelaborde-Augas M. Automatic tool-based pre-processing of generic structural models for water impact simulations in the aircraft pre-design. IOP Conf Ser: Mater Sci Eng 2022;1226:012042. http://dx.doi.org/10.1088/1757-899X/1226/1/012042.
[43] Leon Muñoz C, Kohlgrüber D, Petsch M. High fidelity full aircraft simulations for the application in an industrialized ditching analysis process. In: AIAA Aviation Forum and Ascend. 2024, http://dx.doi.org/10.2514/6.2024-4049.
[44] Schwarz H, Überrück M, Zemke J-PM, Rung T. Machine learning based prediction of ditching loads. AIAA J 2025;63(5):1835–54. http://dx.doi.org/10.2514/1.J064086.
[45] Varmint al's engineering page. 2025, URL http://www.varmintal.com/aengr.htm. (Accessed 10 September 2025).
[46] Vitali E, Benson DJ. An extended finite element formulation for contact in multi-material arbitrary Lagrangian–Eulerian calculations. Internat J Numer Methods Engrg 2006;67(10):1420–44. http://dx.doi.org/10.1002/nme.1681.
[47] Ansys. LS-DYNA user manual. 2024, URL https://ftp.lstc.com/anonymous/outgoing/web/ls-dyna_manuals/R15/LS-DYNA_Manual_Volume_I_R15.pdf.
[48] Van Leer B. Towards the ultimate conservative difference scheme. IV. A new approach to numerical convection. J Comput Phys 1977;23(3):276–99. http://dx.doi.org/10.1016/0021-9991(77)90095-X.
[49] Olovsson L. Training class in ALE and fluid-structure interaction. 2006, URL https://ftp.lstc.com/anonymous/outgoing/support/FAQ_docs/ALE_training_by_Lars.Sept06.pdf.
[50] Ansys. LS-Dyna theory manual. 2024, URL https://ftp.lstc.com/anonymous/outgoing/web/ls-dyna_manuals/DRAFT/DRAFT_Theory.pdf.
[51] Benson DJ. An efficient, accurate, simple ale method for nonlinear finite element programs. Comput Methods Appl Mech Engrg 1989;72(3):305–50. http://dx.doi.org/10.1016/0045-7825(89)90003-0.
[52] Chen H, Do I. Recent development in LS-Dyna S-ALE. In: 15th international LS-DYNA users conference. 2018, URL https://www.dynalook.com/conferences/15th-international-ls-dyna-conference/fsi-ale/recent-developments-in-ls-dyna-r-s-ale.
[53] Chen H. *ALE_STRUCTURED_FSI, the new ALE FSI solver. In: 16th international LS-DYNA users conference. 2020, URL https://www.dynalook.com/conferences/16th-international-ls-dyna-conference/fsi-ale-computing-technology-t8-1/t8-1-b-fsi-ale-081.pdf.
[54] Chen H. LS-Dyna S-ALE recent progress. In: 16th LS-dyna forum. 2022, URL https://www.dynamore.de/de/fortbildung/konferenzen/vergangene/16-ls-dyna-forum-2022/094_chen_ansys.pdf.
[55] Ansys LS-DYNA Aerospace Working Group. Modelling guidelines document, version 25-1, Technical Report. 2025, URL https://awg.ansys.com/MGD.
[56] Chianchiano SM, Colamartino I, Scampini L, Anghileri M. Numerical modelling strategies of fluid-structure interaction for helicopter ditching. In: 5th Aerospace Structural Impact Dynamics International Conference (ASIDIC). 2022.
[57] Ray MH, Mongiardini M, Plaxico CA, Anghileri M. Recommended procedures for verification and validation of computer simulations used for roadside safety applications. In: National Cooperative Highway Research Program (NCHRP), Transportation Research Board of the National Academies of Sciences, Engineering, and Medicine. 2011, URL https://nap.nationalacademies.org/catalog/17647/procedures-for-verification-and-validation-of-computer-simulations-used-for-roadside-safety-applications.
[58] Schwer LE. Validation metrics for response time histories: Perspective and case studies. Eng Comput 2007;23:259–309. http://dx.doi.org/10.1007/s00366-007-0070-1.
[59] Viana Lozoya J, Pastor García G, Climent Máñez H. Flexible structures response to ditching loads. In: presented at the 3rd Aerospace Structural Impact Dynamics International Conference (ASIDIC). Zenodo; 2017, http://dx.doi.org/10.5281/zenodo.1287826.
[60] Yu Z. Water impact damage considering hydro-plastic interactions: Extensive experimental and numerical validation, and structural design recommendations. Mar Struct 2025;101:103766. http://dx.doi.org/10.1016/j.marstruc.2024.103766.
[61] Clevenger RL, Melberg LC. Slamming of a ship structural model. (Master's Thesis), Massachussets Institute of Technology (MIT); 1963.
[62] Abrahamsen BC, Alsos HS, Aune V, Fagerholt E, Faltinsen OM, Hellan Ø. Hydroplastic response of a square plate due to impact on calm water. Phys Fluids 2020;32(8). http://dx.doi.org/10.1063/5.0013858.
[63] Katsuno ET, el Moctar O. Hydroelastoplasticity in helicopter ditching using strongly coupled two-way fluid-structure interaction. Aerosp Sci Technol 2025;110595. http://dx.doi.org/10.1016/j.ast.2025.110595.
[64] Hosseinzadeh S, Tabri K, Topa A, Hirdaris S. Slamming loads and responses on a non-prismatic stiffened aluminium wedge: Part II. Numerical simulations. Ocean Eng 2023;279:114309. http://dx.doi.org/10.1016/j.oceaneng.2023.114309.
[65] Stenius I, Rosén A, Kuttenkeuler J. Hydroelastic interaction in panel-water impacts of high-speed craft. Ocean Eng 2011;38(2–3):371–81. http://dx.doi.org/10.1016/j.oceaneng.2010.11.010.
[66] Nicolosi G, Valpiani F, Grilli G, Saponaro Piacente A, Di Ianni L, Cestino E, Sapienza V, Polla A, Piana P. Design of a vertical ditching test. In: Proc. 32nd ICAS Congress. 2021, p. 6–10, URL https://www.icas.org/icas_archive/ICAS2020/data/papers/ICAS2020_0763_paper.pdf.
[67] Leon Muñoz C, Wegener E, Petsch M, Kohlgrüber D. Detailed FE aircraft fuselage sections for water impact simulations in the pre-design process chain. J Phys: Conf Ser 2023;2526(1):012038. http://dx.doi.org/10.1088/1742-6596/2526/1/012038.
[68] Tay Y, Bhonge P, Lankarani H. Crash simulations of aircraft fuselage section in water impact and comparison with solid surface impact. Int J Crashworthiness 2015;20(5):464–82. http://dx.doi.org/10.1080/13588265.2015.1033972.
[69] Song Y, Horton B, Bayandor J. Verified fuselage section water impact modelling. Aeronaut J 2019;123(1268):1740–54. http://dx.doi.org/10.1017/aer.2019.110.
[70] European union aviation safety agency (EASA), Easy Access Rules for Large Rotorcraft (CS-29). 2023, URL https://www.easa.europa.eu/en/document-library/easy-access-rules/easy-access-rules-large-rotorcraft-cs-29#group-publications.
[71] Rose YA, Oord D, Davis K, Morgan K, Witkowski C. Aviation rulemaking advisory committee (ARAC), Transport aircraft crashworthiness and ditching working group report to FAA. 2018, URL https://www.faa.gov/regulations_policies/rulemaking/committees/documents/index.cfm/document/information/documentID/3743.
[72] Giustina A, Colamartino I, Scampini L, Astori P, Anghileri M. Design and testing of novel three-dimensional modular negative stiffness honeycomb structures as reusable crash absorbers. Int J Crashworthiness 2025;30(3):283–93. http://dx.doi.org/10.1080/13588265.2024.2376796.
[73] Cho J, Lee ES, Kim JH, Lee C-Y, Cho JY. Design of lattice-based energy-absorbing structure for enhancing the crashworthiness of advanced air mobility. Aerospace 2025;12(4). http://dx.doi.org/10.3390/aerospace12040332.